Updip and Along-Strike Aftershock Migration Model Driven by Afterslip: Application to the 2011 Tohoku-Oki Aftershock Sequence

H. Perfettini[1] [ID] **, W. B. Frank[2]** [ID] **, D. Marsan[1]** [ID] **, and M. Bouchon[1]** [ID]

[1]Université Grenoble-Alpes, IRD, CNRS, IFSTTAR, ISTerre, Grenoble, France, [2]Department of Earth Sciences, University of Southern California, Los Angeles, CA, USA

Abstract We present an analytical model based on the idea that afterslip drives seismicity: aftershocks occur when a given level of afterslip is reached in their vicinity. Afterslip is assumed to be governed by a resisting stress that increases as the logarithm of the sliding velocity. This model extends the aftershock migration model of Perfettini et al. (2018, https://doi.org/10.1002/2017GL076287), limited to along-strike migration and the early postseismic phase, to any migration direction (in particular the along-dip migration) and any time of the postseismic phase. This model is able to capture most of the features of aftershock migration such as the increase of the aftershock region as the logarithm of time and the observed aftershock migration velocities. When applied to the aftershock sequence of the Tohoku-Oki earthquake, our model is able to describe the expansion of the aftershock region in both strike and dip directions together with the observed variations of migration velocities.

Plain Language Summary Aftershocks are shown to migrate with time away from the rupture area of the mainshock. We present here a model based on the idea that afterslip drives aftershocks. The model is able to predict observed aftershock migrations both along the strike and dip directions of the fault. We show that the aftershock zone expand as the logarithm of time and predict apparent propagation velocities consistent with the observations. The model is able to explain most of the features of the aftershock sequence of the Tohoku-Oki earthquake.

1. Introduction

Aftershock zones are known to expand with time (e.g.,Chatelain et al., 1983; Henry & Das, 2001; Tajima & Kanamori, 1985) and a migration of the aftershock zone as the logarithm of time has been widely reported (Frank et al., 2017; Kato & Obara, 2014; Meng & Peng, 2016; Obana et al., 2014; Peng & Zhao, 2009; Tang et al., 2014; Wesson, 1987). Perfettini et al. (2018) presented an analytical model of how aftershocks migrate along strike once driven by a mainshock. In this paper, we extend this model to consider along-dip variations of coseismic stress changes and rheological properties to derive a model of aftershock migration in both the along-strike and along-dip directions. Our model predictions are compared to the geometric features and spatial evolution of aftershocks of the 2011 $M_w 9.0$ Tohoku-Oki earthquake. We find that our model predicts the first-order observables of the aftershock expansion.

Thermally activated deformation mechanisms are characterized by an activation rate $v = v_* \exp(\tau \Omega / k_b T)$ where τ is the shear stress acting on the elementary (or activation) volume Ω, k_b is Boltzmann's constant, T is absolute temperature and v_* a reference activation rate. Consequently, the average velocity V of the macroscopic interface or volume considered will be proportional to v so that $V = V_* \exp(\tau \Omega / k_b T)$ where V_* is a reference velocity. This last relation could be written as $\tau = A \log(V/V_*)$ with $A = \Omega / k_b T > 0$. This type of rheology is referred to as a rate strengthening rheology and will be considered in this paper to govern the evolution of afterslip. This process corresponds to a wide range of elementary deformation mechanisms such as rate and state friction, dislocation creep, diffusion creep, pressure solution creep, and stress corrosion, all showing to some extent this type of logarithmic increase of the resisting stress with increasing deformation rate.

Assuming that the frictional stress increases as the logarithm of the sliding rate, Perfettini and Avouac (2004) showed that the temporal evolution of afterslip $U(t)$ is given by

$$U(t) = V_L t_r \log \left[1 + \frac{V_+}{V_L} \left(\exp \left(\frac{t}{t_r} \right) - 1 \right) \right] \qquad (1)$$

where V_L is the long-term sliding (or loading) velocity after the mainshock, V_+ the sliding velocity right after the end of coseismic rupture, and t_r the duration of the postseismic phase. The parameters t_r and V_+ are given by

$$t_r = \frac{A}{\dot{\tau}} \qquad (2a)$$

$$V_+ = V_L \exp \left(\frac{\Delta \text{CFS}}{A} \right) \qquad (2b)$$

where $\dot{\tau}$ and ΔCFS are respectively the stressing rate and Coulomb stress change (induced by the mainshock) on the rate strengthening region. The rheological parameter $A > 0$ is defined as $A = \frac{d\tau_r}{d \log V}$, where τ_r is the resisting stress opposed to motion, which can be related to any thermally activated processes (see Perfettini et al., 2018, for a discussion). The parameter A is assumed here to vary only with temperature and thus depth. If one considers the particular case where the rate strengthening rheology corresponds to rate and state strengthening friction under steady state sliding, then $A = (a - b)\sigma > 0$, where a and b are the rate and state parameters and σ is the effective normal stress(Perfettini & Avouac, 2004).

The sliding velocity $V(t) = \frac{dU}{dt}$ can be obtained using equation (1) giving

$$V(t) = \frac{V_+ \exp \left(\frac{t}{t_r} \right)}{1 + \frac{V_+}{V_L} \left[\exp \left(\frac{t}{t_r} \right) - 1 \right]} \qquad (3)$$

We assume that afterslip is the main mechanism to load the asperities in the postseismic period, producing aftershocks (Perfettini & Avouac, 2004). We speculate that the aftershocks directly triggered by coseismic stress changes only occur in the early stage of the postseismic phase (during, say, the first hours following the mainshock).

The simplest assumption that could be made is that the seismicity rate $R(t)$ in a given area is proportional to the rate of afterslip $V(t)$ at the same location (Perfettini & Avouac, 2004, 2007). After use of equation (3), the seismicity rate is given by

$$R(t) = \frac{R_+ \exp \left(\frac{t}{t_r} \right)}{1 + \frac{R_+}{R_L} \left[\exp \left(\frac{t}{t_r} \right) - 1 \right]} \qquad (4)$$

where R_L is the long-term seismicity rate after the mainshock, R_+ the seismicity rate at the end of coseismic rupture, and t_r the duration of the postseismic phase. The parameter R_+ is given by

$$R_+ = R_L \exp \left(\frac{\Delta \text{CFS}}{A} \right) \qquad (5)$$

2. Estimate of the Aftershock Migration Velocity Assuming an Afterslip Threshold

2.1. Model Assumptions

We consider a fault with only depth-varying properties so that the normal stress, stressing rate, and rheological parameter A can change with depth but are assumed to be laterally uniform (along strike).

Figure 1 taken from Perfettini et al. (2018) shows a schematic sketch of the model. During the interseismic phase (Figure 1a), a population of asperities (dark blue patches) are loaded by the surrounding interseismic creep (yellow region), occurring at a steady state velocity. When the mainshock occurs (Figure 1b), some asperities slip coseismically (red patches), transferring large positive Coulomb stress into the nearby creeping regions. During the postseismic phase (Figure 1c), the creeping regions loaded by the mainshock experience large amounts of afterslip (orange region). As this afterslip increases along the fault with time, aftershocks (light blue) are produced accordingly when a significant amount of afterslip accumulates. It is
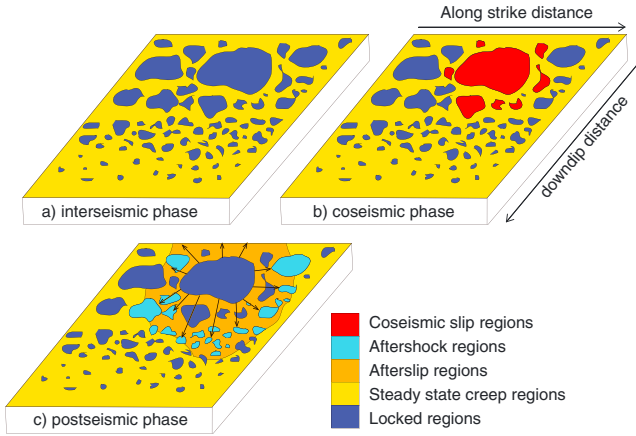
Figure 1. Schematic sketch of the model: (a) during the interseismic phase, a population of asperities (dark blue patches) are loaded by the surrounding interseismic creep (yellow region), occurring at a steady state (plate) velocity; (b) during the coseismic phase, some asperities slip coseismically (red patches), transferring large positive Coulomb stress into the nearby creeping regions; (c) during the postseismic phase, the creeping regions loaded by the mainshock show large amount of afterslip (orange region). As this afterslip increases along the fault with time, aftershocks (light blue) are produced accordingly when a significant amount of afterslip (of the order of $U_a = V_L t_r$ where V_L is the plate velocity and t_r the duration of the aftershock sequence; see Perfettini et al., 2018, for more details) is reached. The black vectors describe the afterslip migration.

important to stress that afterslip is initiated directly after the coseismic rupture in every rate strengthening region of the fault plane and that its accumulation rate is strongly dependent on the initial coseismic stress field (and hence on the distance from the rupture). Therefore, afterslip migration is purely apparent.

Because of our model assumptions, we consider solely the aftershocks located near the regions with large amount of afterslip. Those regions are expected to be located near the rupture zone, say, within a rupture length from the rupture area. Therefore, our model intends to model the aftershock migration in the vicinity of the rupture area and cannot explain remotely triggered aftershocks.

We define the aftershock migration as the velocity with which the spatial aftershock coverage grows. We refer to this expanding region as the aftershock zone. We will consider the migration of aftershocks along the strike and dip direction x and z and assume the following variable dependencies: $\dot{\tau}(z)$, $A(z)$, $t_r(z)$, $\Delta CFS(x, z)$ and $V_+(x, z)$. With those assumptions, equations (1) and (3) read

$$U(x, z; t) = V_L t_r(z) \log D(x, z; t) \tag{6a}$$

$$V(x, z; t) = \frac{V_+(x, z) \exp\left(\frac{t}{t_r(z)}\right)}{D(x, z; t)} \tag{6b}$$

$$D(x, z; t) = 1 + \frac{V_+(x, z)}{V_L} \left[\exp\left(\frac{t}{t_r(z)}\right) - 1\right] \tag{6c}$$

In our model, aftershocks are produced when a given level of afterslip is reached in their surrounding. Perfettini et al. (2018) showed that this level was of the order of $V_L t_r$ (where $V_L \ll V_+$), which represents the slip that would be accumulated during the total duration t_r of the postseismic period assuming sliding at the plate velocity. Note that the long-term velocity might be different from the plate velocity due to the pinning effects of asperities on the nearby creeping regions, as expected in "Chilean"-type subduction zones in the sense of Tajima and Kanamori (1985). Therefore, V_L must be seen as a long-term creeping velocity averaged over a region large enough to avoid those local effects and could be significantly different from the plate velocity. Similarly, the afterslip threshold level has to be seen as an average value over the region of interest. Note that in the rest of the derivation, the only assumption is that a constant afterslip level is reached but its precise value has no influence on the model predictions.

Consequently, between time t and $t + \mathrm{d}t$, a constant slip level initially located at position (x, z) at time t is now located at position $(x + \mathrm{d}x, z + \mathrm{d}z)$ given by

$$\mathrm{d}U = \frac{\partial U}{\partial x} \mathrm{d}x + \frac{\partial U}{\partial z} \mathrm{d}z + \frac{\partial U}{\partial t} \mathrm{d}t = 0 \tag{7}$$

For a fixed depth z, equation (7) becomes

$$\frac{\partial U}{\partial x} \mathrm{d}x + \frac{\partial U}{\partial t} \mathrm{d}t = 0 \tag{8}$$

and the along-strike migration velocity $V_p^x = \frac{\mathrm{d}x}{\mathrm{d}t}$ is given by

$$V_p^x = \frac{-V}{\frac{\partial U}{\partial x}} \tag{9}$$

with the use of the definition $V \equiv \frac{\partial U}{\partial t}$.

For a fixed along-strike position x, a similar calculation gives the updip migration velocity $V_p^z = \frac{\mathrm{d}z}{\mathrm{d}t}$

$$V_p^z = \frac{-V}{\frac{\partial U}{\partial z}} \tag{10}$$

2.2. Along-Strike Aftershock Migration Velocity

In Appendix A2, equation (A10) gives the along-strike aftershock migration velocity given by

$$V_p^x(x, z; t) = \frac{A(z)}{F(z; t)t_r(z)} \times \left(-\frac{\partial \Delta CFS(x, z)}{\partial x} \right)^{-1} \tag{11}$$

where

$$F(z; t) = \left[1 - \exp\left(-t/t_r(z) \right) \right] \tag{12}$$

Considering the limit of small times ($t \ll t_r$), equation (11) becomes, after use of (A11a),

$$V_p^x = \frac{A}{t} \times \left(-\frac{\partial \Delta CFS}{\partial x} \right)^{-1}, t \ll t_r \tag{13}$$

which is identical to equation (17) of Perfettini et al. (2018), obtained considering the limit $t \ll t_r$, equivalent to the limit $t \to 0$ of equation (A11a).

2.3. Updip Aftershock Migration Velocity

In Appendix A3, equation (A21) gives the updip aftershock migration velocity

$$V_p^z(x, z; t) = \frac{A(z)}{F(z; t)t_r(z)} \times \left[\left(\frac{1}{A(z)} \frac{\partial A(z)}{\partial z} \right) \Delta CFS(x, z) + \left(\frac{-\partial \Delta CFS(x, z)}{\partial z} \right) \right]^{-1} \tag{14}$$

where F was defined in equation (12).

The ratio of the two terms within the brackets of the denominator of equation (14) is $\left(\frac{1}{A} \frac{\partial A}{\partial z} \right) \Delta CFS / \left(\frac{-\partial \Delta CFS}{\partial z} \right)$, which is of the order of $\left(\frac{\delta A}{A} \right) / \left(\frac{-\delta \Delta CFS}{\Delta CFS} \right)$ where δA and $\delta \Delta CFS$ are respectively the characteristic variations of A and ΔCFS with depth.

In the case of the Illlapel earthquake, we find using Figure 4A of Frank et al. (2017) that the relative change of the A parameter (named A' in Frank et al., 2017) between 10- and 40-km depths is of the order of $|\delta A/A| \approx 0.15$, while the Coulomb stress distribution of Figure S4 of Frank et al. (2017) is of the order of $|\delta \Delta CFS/\Delta CFS| \approx 0.25$. Even though $|\delta \Delta CFS/\Delta CFS|$ is found to be larger than $|\delta A/A|$ based on the results of Frank et al. (2017), the relative variations of A are not negligible compared to those of the coseismic Coulomb stress changes. Nevertheless, the derivation of the distribution of the A parameter with depth obtained in Frank et al. (2017) relies on the assumed Coulomb stress field, which is certainly a smoothed version of the real Coulomb stress field (that could be much rougher as small scale heterogeneities can not be accounted for in kinematic slip inversions). Therefore, we assume that the gradient in Coulomb stress has a much larger amplitude than the A parameter gradient.

Under the assumption that the relative variations of the rheological parameter A with depth are negligible compared to the relative changes in Coulomb stress associated with coseismic slip, equation (14) simplifies into

$$V_p^z(x, z; t) \approx \frac{A(z)}{F(z; t)t_r(z)} \times \left(\frac{-\partial \Delta CFS(x, z)}{\partial z} \right)^{-1} \tag{15}$$

which has a form similar to equation (11) for the along-strike aftershock migration velocity.

In the limit $t \ll t_r$, equation (12) shows that $F(z; t) \approx t/t_r$ so that equation (15) yields

$$V_p^z(x, z; t) \approx \frac{A(z)}{t} \times \left(\frac{-\partial \Delta CFS(x, z)}{\partial z} \right)^{-1} \tag{16}$$

2.4. General Expression of the Aftershock Migration Velocity

The aftershock migration velocity vector $\vec{V}_p$ has components V_p^x in the along-strike direction and V_p^z in the along-dip direction. Therefore, the amplitude V_p of the velocity vector $\vec{V}_p$ is given by

$$V_p = \sqrt{(V_p^x)^2 + (V_p^z)^2} \tag{17}$$

Using equations (11) and (15), equation (17) becomes

$$V_p(x, z; t) = \frac{A(z)}{F(z; t)t_r(z)} \sqrt{\left(-\frac{\partial \Delta CFS(x, z)}{\partial x} \right)^{-2} + \left(\frac{-\partial \Delta CFS(x, z)}{\partial z} \right)^{-2}} \tag{18}$$

If L_x and L_z are respectively the along-strike and downdip extent of coseismic rupture with associated stress drop $\Delta\tau$, then a simplified form of equation (18) is given by

$$V_p(x, z; t) \approx \frac{A(z)}{F(z; t)t_r(z)\Delta\tau} \sqrt{L_x^2 + L_z^2} \tag{19}$$

Since $F(z; t) \approx t/t_r$ for $t \ll t_r$, equation (19) yields

$$V_p(z; t) \approx \frac{A(z)}{t} \times \frac{\sqrt{L_x^2 + L_z^2}}{\Delta\tau}, \, t \ll t_r \tag{20}$$

In the approximation of the aftershock migration velocity given in equation (20), V_p only depends on depth through the depth dependence of the rheological parameter A. Equation (20) is similar to equation (23) derived in Perfettini et al. (2018), which considered the along-strike aftershock migration velocity alone.

Small to moderate earthquakes only rupture a small fraction of the seismogenic zone and the crude assumption of a circular rupture might be appropriate. In this case, $L_x = L_y$ and following Perfettini et al. (2018), equation (19) can be written as

$$V_p(x, z; t) \approx \zeta \frac{A(z)}{F(z; t)t_r(z)} \frac{r}{\Delta\tau} \tag{21}$$

where ζ is a shape factor of order unity. If we impose the rupture area of the rectangular and circular model of radius r to be identical so that $L_x L_y = L_x^2 = \pi r^2$, then $\zeta = \sqrt{2\pi}$. Large earthquakes rupture the entire width W of the seismogenic zone so that $L_z \approx W$ while L_x corresponds to the along-strike extent of rupture. When considering those type of events, the circular rupture assumption is no longer appropriate and equation (20) should be used.

In the limit $t \gg t_r$, equation (A11b) combined with (21) leads to

$$V_p(x, z) \equiv V_p^\infty \approx \zeta\dot{\tau} \frac{r}{\Delta\tau}, \, t \gg t_r \tag{22}$$

where the definition $t_r \equiv A/\dot{\tau}$ has been used. Noting that $\Delta\tau/\dot{\tau} = T_{\mathrm{rec}}$ corresponds to the recurrence (or return) time of the earthquake, equation (22) becomes

$$V_p^\infty \approx \zeta \frac{r}{T_{\mathrm{rec}}} \tag{23}$$

Based on equation (23), the minimum propagation velocity V_p^∞, reached at the end of the aftershock sequence, would be of the order of 1 km/year for a rupture radius of 100 km and a recurrence time of 100 years. Note that according to equation (23), V_p^∞ is of the order of $\frac{r}{T_{\mathrm{rec}}}$, which corresponds to a migration over the entire rupture area during the entire interseismic period.

3. Estimate of the Aftershock Migration Velocity Assuming the Seismicity Model of Perfettini and Avouac (2004)

We present here an alternate derivation of the aftershock migration velocities based on the seismicity model of Perfettini and Avouac (2004). The correspondence between this model and the afterslip threshold model of section 2 is discussed in section 3.3.

According to the afterslip-driven seismicity model of Perfettini and Avouac (2004), the seismicity rate jumps from a long-term value R_L prior to the mainshock to a value R_+ immediately at the end of the coseismic phase. The seismicity rate R then remains nearly constant ($R \approx R_+$) during a period t_a given by

$$t_a = \exp\left(-\frac{\Delta\mathrm{CFS}}{A}\right) t_r \tag{24}$$

after which $R(t)$ decays as 1/time before getting back to the steady state value R_L at the end of the aftershock sequence of duration t_r.

According to the variable dependencies of our model (section 2.1), Equation (24) can be written as

$$t_a(x, z) = \exp\left(-\frac{\Delta\mathrm{CFS}(x, z)}{A(z)}\right) t_r(z) \tag{25}$$

3.1. Along-Strike Aftershock Migration Velocity

Differentiating equation (25) with respect to the along-strike distance x gives

$$\frac{\partial t_a}{\partial x} = -\frac{t_a}{A}\frac{\partial \Delta \mathrm{CFS}}{\partial x} \tag{26}$$

Following Perfettini et al. (2018), the propagation velocity $V_p^x = \frac{\partial x}{\partial t_a}$ can be obtained using equation (26) yielding

$$V_p^x(x,z;t) = \frac{A(z)}{t} \times \left(-\frac{\partial \Delta \mathrm{CFS}(x,z)}{\partial x}\right)^{-1} \tag{27}$$

which corresponds to equation (12) of Perfettini et al. (2018). Equation (27) is identical to equation (13) derived assuming an afterslip threshold.

3.2. Updip Aftershock Migration Velocity

Differentiating equation (25) with respect to the updip distance z gives

$$\frac{1}{t_a}\frac{\partial t_a}{\partial z} = \left[\frac{1}{t_r}\frac{\partial t_r}{\partial z} - \frac{\partial}{\partial z}\left(\frac{\Delta \mathrm{CFS}}{A}\right)\right] \tag{28}$$

Combining equation (28) with (A15) leads to

$$\frac{1}{t_a}\frac{\partial t_a}{\partial z} = \left[\frac{1}{A}\frac{\partial A}{\partial z}\left(1 + \frac{\Delta \mathrm{CFS}}{A}\right) - \frac{1}{\dot{\tau}}\frac{\partial \dot{\tau}}{\partial z} - \frac{1}{A}\frac{\partial \Delta \mathrm{CFS}}{\partial z}\right] \tag{29}$$

The updip aftershock migration velocity $V_p^z = \frac{\partial z}{\partial t_a}$ can be obtained using equation (29) yielding

$$V_p^z(x,z;t) = \frac{A(z)}{t} \times \left[\frac{\partial A(z)}{\partial z}\left(1 + \frac{\Delta \mathrm{CFS}(x,z)}{A(z)}\right) - t_r(z)\frac{\partial \dot{\tau}(z)}{\partial z} - \frac{\partial \Delta \mathrm{CFS}(x,z)}{\partial z}\right]^{-1} \tag{30}$$

where $t_r = A/\dot{\tau}$ has been used.

If we assume that the variations of stressing rate $\dot{\tau}$ and rheological parameter A are moderate with depth such that the term $\frac{\partial \Delta \mathrm{CFS}}{\partial z}$ dominates the other within the brackets of equation (30), equation (30) simplifies into

$$V_p^z(x,z;t) \approx \frac{A(z)}{t} \times \left(-\frac{\partial \Delta \mathrm{CFS}(x,z)}{\partial z}\right)^{-1} \tag{31}$$

which is identical to equation (15) when $F(z;t) = t/t_r$, which corresponds to the limit $t \ll t_r$ of equation (15).

3.3. Correspondence Between the Afterslip Threshold Level and the Afterslip-Driven Seismicity Model

Equations (13) and (16) obtained considering the afterslip threshold model of section 2 are respectively identical to equations (27) and (31) obtained in section 3 considering the afterslip-driven seismicity model of Perfettini and Avouac (2004). The same exact correspondence between both models has been previously evidenced by Perfettini et al. (2018) considering only the along-strike aftershock migration in the early times of the postseismic phase ($t \ll t_r$).

The agreement between both models was obtained considering the results of section 2 in the limit $t \ll t_r$ so that the results of the afterslip driven seismicity model of section 3 can be seen as an approximation at early times of the more general derivation of section 2. Indeed, the results of section 3 relies on the expression of the characteristic aftershock duration t_a, which was derived considering the intersection of the constant seismicity rate R_+ right after the mainshock with the evolution of the seismicity rate following an infinite step in Coulomb stress (see Appendix A of Perfettini et al., 2018, for more details). The approximation of a constant seismicity rate R_+ (corresponding to the size of the aftershock zone) is only valid when $t \ll t_r$ and so are the evaluations of the aftershock migration velocities of section 3.

Note that equations (14) and (30) are identical when $F = t/t_r$ (corresponding to the approximation $t \ll t_r$), $\frac{\partial \dot{\tau}}{\partial z} = 0$, and $\Delta \mathrm{CFS} \gg A$, an approximation that seems reasonable in the case of the Illapel earthquake where $\Delta \mathrm{CFS} \approx 0.27$ MPa and $A \approx 3.7 \times 10^{-2}$ MPa (Frank et al., 2017).

3.4. Expansion of the Aftershock Zone

Between time t_1 and $t_2 > t_1$, equations (11) and (15) show that the aftershock region has expanded of amount Δx_p given by

$$\Delta X_p^x(x, z; t_1, t_2) = \frac{A(z)}{t_r(z)} \times \left(-\frac{\partial \Delta\text{CFS}(x, z)}{\partial x}\right)^{-1} \times \int_{t_1}^{t_2} \frac{1}{F(t')} \, dt' \tag{32a}$$

$$\Delta X_p^z(x, z; t_1, t_2) = \frac{A(z)}{t_r(z)} \times \left(\frac{-\partial \Delta\text{CFS}(x, z)}{\partial z}\right)^{-1} \times \int_{t_1}^{t_2} \frac{1}{F(t')} \, dt' \tag{32b}$$

Using equation (12), we have

$$\int_{t_1}^{t_2} \frac{1}{F(t')} \, dt' = \int_{t_1}^{t_2} \frac{\exp\left(t'/t_r(z)\right)}{\exp\left(t'/t_r(z)\right) - 1} \, dt' = t_r(z) \times \log\left[\frac{\exp\left(t_2/t_r(z)\right) - 1}{\exp\left(t_1/t_r(z)\right) - 1}\right] \tag{33}$$

so that equations (32a) give

$$\Delta X_p^x(x, z; t_1, t_2) = A(z) \times \left(-\frac{\partial \Delta\text{CFS}(x, z)}{\partial x}\right)^{-1} \times \log\left[\frac{\exp\left(t_2/t_r(z)\right) - 1}{\exp\left(t_1/t_r(z)\right) - 1}\right] \tag{34a}$$

$$\Delta X_p^z(x, z; t_1, t_2) = A(z) \times \left(\frac{-\partial \Delta\text{CFS}(x, z)}{\partial z}\right)^{-1} \times \log\left[\frac{\exp\left(t_2/t_r(z)\right) - 1}{\exp\left(t_1/t_r(z)\right) - 1}\right] \tag{34b}$$

3.5. Limit of the Aftershock Region in the Limit $t \ll t_r$

As the aftershock production rate decays roughly as the inverse of the time elapsed since the mainshock, aftershocks are numerous only in the early part of the postseismic phase (typically lasting several years). Furthermore, it is shown in Appendix A2 (see Figure A1) that the function F defined in equation (12) (accounting for the temporal evolution of the aftershock region) is well approximated by $F \approx t/t_r$ corresponding to the limit $t \ll t_r$ as long as t is not of the same order as the duration t_r of the aftershock sequence. Consequently, the approximation $t \ll t_r$ is appropriate when studying most aftershock sequences.

In the limit $t \ll t_r$, Equations (34a) and (34b) show that between time t_1 and t_2, the aftershock front has moved of an amount ΔX_p given by

$$\Delta X_p^x(x, z; t_1, t_2) = V_{p/d}^x(x, z) \times \log\left(\frac{t_2}{t_1}\right), \, t \ll t_r \tag{35a}$$

$$\Delta X_p^z(x, z; t_1, t_2) = V_{p/d}^z(x, z) \times \log\left(\frac{t_2}{t_1}\right), \, t \ll t_r \tag{35b}$$

with

$$V_{p/d}^x(x, z) = A(z) \times \left(-\frac{\partial \Delta\text{CFS}(x, z)}{\partial x}\right)^{-1} \tag{36a}$$

$$V_{p/d}^z(x, z) = A(z) \times \left(\frac{-\partial \Delta\text{CFS}(x, z)}{\partial z}\right)^{-1} \tag{36b}$$

where $V_{p/d}$ (which has the dimension of a distance) is often found in the literature as the migration velocity per decade.

Equations (35a) and (35b) will be used to study the aftershock sequence of the Tohoku-Oki earthquake. Note that according to our model, the parameter that characterizes alone the amplitude of the aftershock migration is $V_{p/d}$.

4. Application to the Aftershock Migration of the 2011 M_w9.0 Tohoku-Oki Earthquake

We study here the along-strike and updip aftershock migration of the Tohoku-Oki earthquake, considering all $M_w > 2$ aftershocks located less than 20 km away from the fault geometry of Hayes et al. (2012). Note
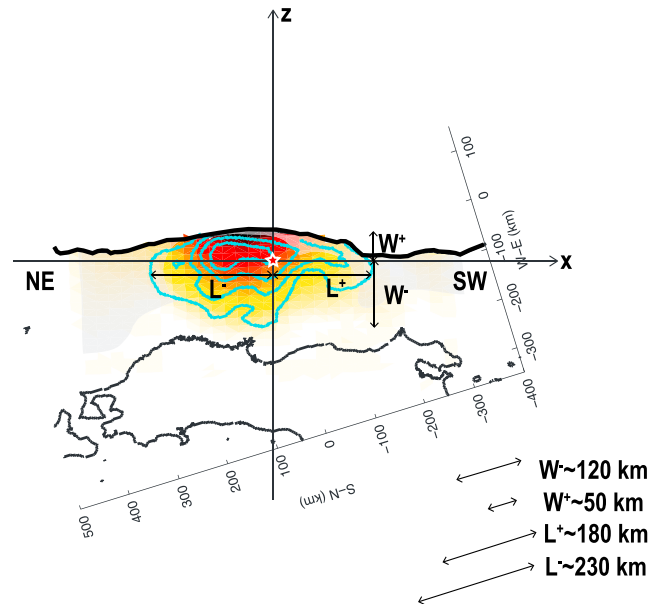
Figure 2. Coseismic slip distribution of the Tohoku-Oki earthquake from Wei et al. (2012; cyan contours) and Perfettini and Avouac (2014; color map; modified from Figure 5 of Perfettini & Avouac, 2014). The coordinate frame used in this study is centered on the earthquake hypocenter (white star) and is defined by the x axis (oriented along the mean strike of the fault) and the z axis (oriented along the mean dip direction). Coseismic rupture extended left and right from the hypocenter by an amount $L^- \approx 230$ km and $L^+ \approx 180$ km and propagated downdip and updip from the hypocenter by an amount $W^- \approx 120$ km and $W^+ \approx 50$ km.

that the cutoff magnitude is larger than the completeness magnitude of the Japanese Meteorological Agency catalog used in this study, which is of the order of 1 (Nanjo et al., 2010).

Figure 2 shows the coseismic slip distribution of Wei et al. (2012) and Perfettini and Avouac (2014) together with the coordinate axis (x, z) used to derive the along-strike and updip migration velocities. Based on those coseismic models, the coseismic rupture extended left and right from the hypocenter by the respective amounts of $L^- \approx 230$ km and $L^+ \approx 180$ km, while it extended downdip and updip by the respective amounts of $W^- \approx 120$ km, $W^+ \approx 50$ km. Consequently, the total along-strike extent of rupture is $L_{tot} = L^+ + L^- \approx 410$ km and the total downdip dimension of rupture is $W_{tot} = W^+ + W^- \approx 170$ km. These values will be later used when comparing the model with the observations.
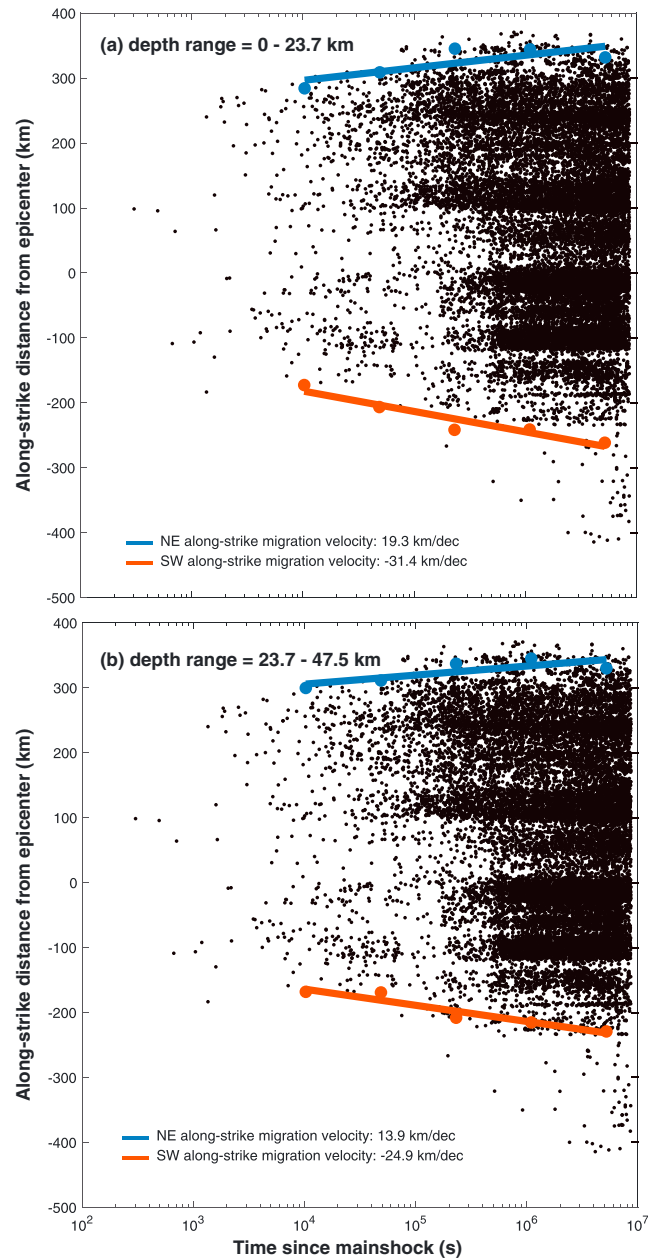
The along-strike and updip aftershock migration are obtained considering respectively the temporal evolution of the along-strike and along-dip coordinates (see Appendix B). We consider two depth slices: the shallower slice corresponds to the depth range $[0; d_e]$ and the second one to the depth range $[d_e; 2d_e]$ where $d_e = 23.7$ km is the hypocenter depth. For each depth slice, the temporal evolution is studied considering five time intervals ranging from 1 hr to 100 days, with a logarithmic increment. Those parameters values were chosen to insure a sufficient number of aftershocks to evaluate the migration velocity $V_{p/d}$ given in equations (35a) and (35b). For a given time interval, the limit of the aftershock zone is found considering the quantiles corresponding to 99% of the aftershocks found in this given time interval.

4.1. Along-Strike Aftershock Migration

Figure 3 shows the along-strike aftershock migration following the Tohoku-Oki earthquake in the depth range $[0; d_e]$ (Figure 3a) and $[d_e; 2d_e]$ (Figure 3b). The limit of the aftershock region is defined by the open circles (red: NE limit; blue: SW limit) and the continuous line corresponds to the approximation of equation (35a).

The expansion of the aftershock region above (resp. below) the hypocenter is well described by equation (35a) using $V_{p/d}^x \approx 19.3$ km per decade (resp. 13.9 km per decade) SW from the hypocenter and $V_{p/d}^x \approx 31.4$ km per decade (resp. 24.9 km per decade) NE of it as may be seen on Figure 3a (resp. Figure 3b).
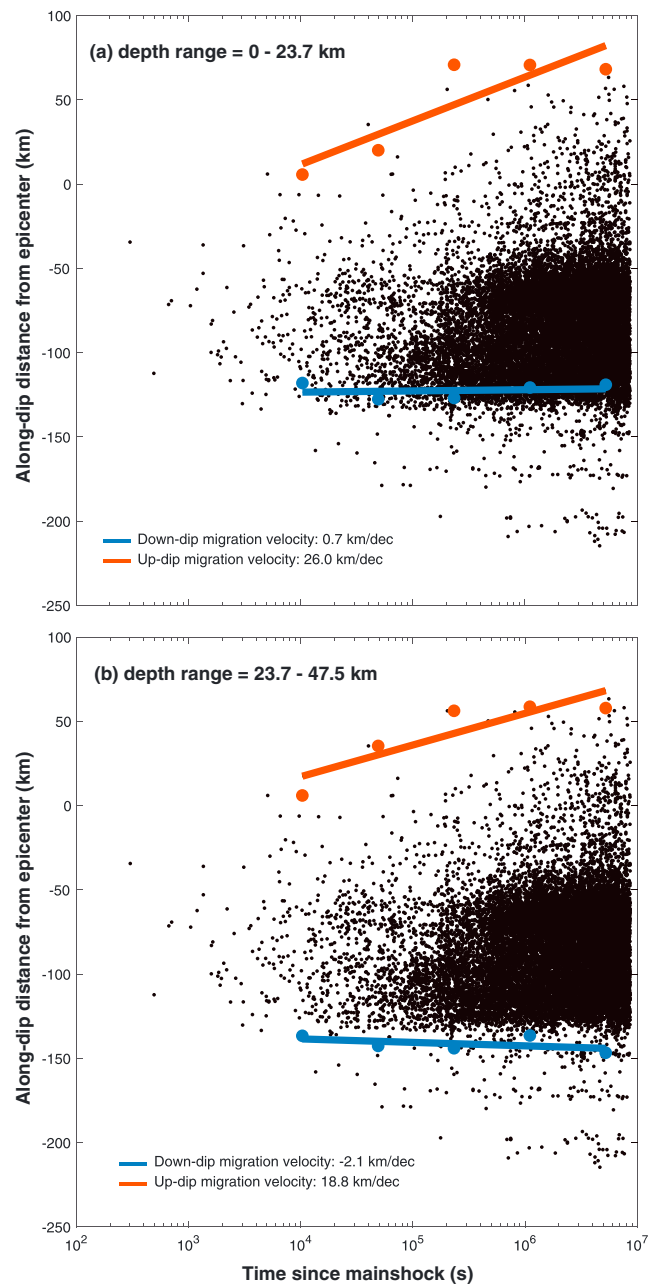
Figure 3. Along-strike aftershock migration following the Tohoku-Oki earthquake: (a) migration in the depth range 0–23.7 km, which corresponds to the aftershocks shallower than the hypocenter. (b) Migration in the depth range 23.7–47.5 km, which corresponds to the aftershocks deeper than the hypocenter. The limit of the aftershock region is defined by the open circles (red: NE limit; blue: SW limit). The continuous line corresponds to the approximation of equation (35a).

Two main features can be noted on Figure 3. First, the migration velocity SW from the hypocenter is larger than NE from it, by a factor $31.4/19.3 \approx 1.63$ above the hypocenter and $24.9/13.9 \approx 1.79$ below it. Second, the migration velocities are larger above the hypocenter then below it, with a factor $19.3/13.9 \approx 1.39$ SW from the hypocenter and $31.4/24.9 \approx 1.26$ NE from it.

4.2. Along-Dip Aftershock Migration

Figure 4 shows the along-dip aftershock migration following the Tohoku-Oki earthquake in the depth range $[0; d_e]$ (Figure 4a) and $[d_e; 2d_e]$ (Figure 4b). The limit of the aftershock region is defined by the open circles (red: updip limit; blue: downdip limit) and the continuous line corresponds to the approximation of equation (35b).

Figure 4. Along-strike aftershock migration following the Tohoku-Oki earthquake: (a) migration in the depth range 0–23.7 km, which corresponds to the aftershocks shallower than the hypocenter. (b) Migration in the depth range 23.7–47.5 km, which corresponds to the aftershocks deeper than the hypocenter. The limit of the aftershock region is defined by the open circles (red: updip limit; blue: downdip limit). The continuous line corresponds to the approximation of equation (35b).

The expansion of the aftershock region above (resp. below) the hypocenter is well described by equation (35b) using $V_{p/d}^z \approx 26.0$ km per decade (resp. 18.8 km per decade) for the updip direction. For the downdip direction, the migration velocity is so low that our algorithm fails to determine them properly. Consequently, we will restrain our analysis to the aftershock migration in the updip direction.

Two main features can be noted on Figure 4. First, the migration velocity in the updip direction is much larger than in the downdip direction. A reliable estimate of the corresponding ratio cannot be made as there is no apparent migration in the downdip direction with a migration velocity in the downdip direction

close to 0. The second remarkable feature of Figure 4 is that the migration velocities are larger above the hypocenter then below it, with a factor $26.0/18.8 \approx 1.38$ in the updip direction. This feature is discussed in the conclusion.

4.3. Discussion

Based on equations (35a) and (35b), and (36a) and (36b), the ratio between $V_{p/d}^{x-}$ left (NE) from the hypocenter and $V_{p/d}^{x+}$ right (SW) from the hypocenter is given by

$$\frac{V_{p/d}^{x-}}{V_{p/d}^{x+}} = \frac{\frac{\partial \Delta \mathrm{CFS}}{\partial x}(x > 0)}{\frac{\partial \Delta \mathrm{CFS}}{\partial x}(x < 0)} \tag{37}$$

It is important to note that the ratio $V_{p/d}^{-}/V_{p/d}^{+}$ does only depend on the ratio of the gradient in Coulomb stress. Based on Figure 2, we can assume that

$$\frac{\partial \Delta \mathrm{CFS}}{\partial x}(x < 0) \approx \frac{-\Delta \tau}{L^{-}} \tag{38a}$$

$$\frac{\partial \Delta \mathrm{CFS}}{\partial x}(x > 0) \approx \frac{-\Delta \tau}{L^{+}} \tag{38b}$$

where L^{-} and L^{+} are respectively the extent of rupture left and right from the epicenter and $\Delta \tau$ the stress drop of the mainshock. Combining equations (37) and (38a) gives

$$\frac{V_{p/d}^{x-}}{V_{p/d}^{x+}} \approx \frac{L^{-}}{L^{+}} \tag{39}$$

Taking $L^{-} \approx 230$ km and $L^{+} \approx 180$ km as estimated from Figure 2 gives $\frac{V_{p/d}^{x-}}{V_{p/d}^{x+}} \approx 1.3$. In section 4.1, we found that the migration velocity $V_{p/d}^{-}$ (NE from the hypocenter) was larger than $V_{p/d}^{+}$ (SW from the hypocenter) by a factor $31.4/19.3 \approx 1.63$ above the hypocenter and $24.9/13.9 \approx 1.79$ below it. As a result, our model predicts that $V_{p/d}^{-}/V_{p/d}^{+} > 1$ and the estimated ratio of the order of 1.3 is consistent with the observations.

A similar procedure can be applied to compare the migration velocities in the along-dip direction below and above the hypocenter. Using equation (36b), we find

$$\frac{V_{p/d}^{z-}}{V_{p/d}^{z+}} = \frac{A(z < 0)}{A(z > 0)} \times \frac{\frac{\partial \Delta \mathrm{CFS}}{\partial z}(z > 0)}{\frac{\partial \Delta \mathrm{CFS}}{\partial z}(z < 0)} \tag{40}$$

Assuming an homogenous stress drop over the rupture zone, equation (40) becomes

$$\frac{V_{p/d}^{z-}}{V_{p/d}^{z+}} \approx \frac{A(z < 0)}{A(z > 0)} \times \frac{W^{-}}{W^{+}} \tag{41}$$

Taking $W^{-} \approx 120$ km and $W^{+} \approx 50$ km as estimated from Figure 2 and assuming that $A(z < 0) \approx A(z > 0)$ gives $\frac{V_{p/d}^{z-}}{V_{p/d}^{z+}} \approx 2.4$. This estimate is in quantitative agreement, although larger, than our estimate of 1.38 derived in section 4.3. A perfect agreement could be reached assuming that $\frac{A(z<0)}{A(z>0)} \approx 1.38/2.4 \approx 0.6$, which would correspond to an increase of the parameter A with depth. Such an increase is consistent with the results of Frank et al. (2017) for the aftershock sequence of the Illapel earthquake (see their Figure 4).

Comparing the results of sections 4.1 and 4.3, it is obvious that the aftershock migration velocities are larger in the along-strike direction than in the dip direction. Considering the highest along-dip migration velocities (corresponding to the updip migration) with the highest along-strike migration velocities gives a ratio of $31.4/26 \approx 1.2$ above the hypocenter and $24.9/18.8 \approx 1.3$ below it. Note that this ratio can be much larger considering the downdip migration velocity as the latter is near 0.

Comparing equations (36a) and (36b) at the same depth range gives

$$\frac{V_{p/d}^{x}}{V_{p/d}^{z}} = \frac{\frac{\partial \Delta \mathrm{CFS}}{\partial z}}{\frac{\partial \Delta \mathrm{CFS}}{\partial x}} \tag{42}$$

where $V^x_{p/d}$ and $V^z_{p/d}$ are respectively the characteristic along-strike and along-dip migration velocities. From dimensional analysis, the following approximation can be made

$$\frac{\partial \Delta \text{CFS}}{\partial x} \approx \frac{\Delta \tau}{L_{\text{tot}}} \tag{43a}$$

$$\frac{\partial \Delta \text{CFS}}{\partial z} \approx \frac{\Delta \tau}{W_{\text{tot}}} \tag{43b}$$

where L_{tot} and W_{tot} are respectively the total along-strike and along-dip extent of the mainshock rupture (see Figure 2). Combining equation (42) with equations (43a) and (43b) yields

$$\frac{V^x_{p/d}}{V^z_{p/d}} \approx \frac{L_{\text{tot}}}{W_{\text{tot}}} \tag{44}$$

Considering $L_{\text{tot}} \approx 410$ km and $W_{\text{tot}} \approx 170$ km as derived from Figure 2 leads to $\frac{V^x_{p/d}}{V^z_{p/d}} \approx 2.4$ is in qualitative agreement with the ratio of 1.2–1.3 found above.

5. Conclusion

We present an analytical model based on the idea that afterslip drives seismicity. When applied to the postseismic period, it is assumed that aftershocks occur when a given level of afterslip is reached in their surrounding. Afterslip is supposed to be governed by a resisting stress that increases as the logarithm of the sliding velocity. This type of rheology may correspond to rate strengthening friction but more generally, to any thermally activated process obeying an Arrhenius law. Deformation mechanisms such as dislocation creep, diffusion creep, pressure solution creep, and even stress corrosion would lead to identical predictions, as discussed in Perfettini et al. (2018).

Our model can describe the migration of aftershocks in the along-strike and dip directions of the fault. As aftershock sequences are usually studied in the early postseismic phase (because of the large deviation of the seismicity rate compared to its steady state level) corresponding to the limit $t \ll t_r$ (where t_r is the duration of the aftershock sequence), most of the analytical expressions are given in the limit $t \ll t_r$. This is the case in the expression of the aftershock migration velocities or dimension of the aftershock zone given respectively in equations (13), (16), and (35a) and (35b), which are approximations of the full expressions given in equations (11), (15), and (34a) and (34b). The latter equations can be used to study the end of the postseismic period and the return of seismicity to its long-term rate, but for most practical use, the approximations given in equations (36a) and (36b), and (35a) and (35b) are relevant.

Our model can explain the main features of the migration of aftershock zones such as the growth of the aftershock zones as the logarithm of time corresponding to a migration rate decaying as 1/time as predicted by equations (13), (16), and (35a) and (35b). It also predicts migration velocities consistent with the observations. Indeed, the speed of the aftershock migration is controlled by the parameter $V_{p/d}$ given in equations (36a) and (36b), which solely depends on the parameter A characterizing the rate strengthening rheology and the inverse of the gradient in coseismic Coulomb stress. Assuming that the gradient of coseismic Coulomb stress can be approximated by $\Delta \tau / r$ where $\Delta \tau$ is the stress drop of the mainshock and r the characteristic size of the rupture zone, the migration velocity per decade $V_{p/d}$ is of the order of $V_{p/d} \approx \zeta A r / \Delta \tau$ where ζ is a shape factor of order unity (a value of $\zeta = \sqrt{2\pi}$ was proposed in section 2.4). Taking $A = 0.1$–1 MPa as previously derived in postseismic studies (e.g., Perfettini et al., 2010, and reference therein), $\Delta \tau = 3$ MPa as characteristic of the earthquake stress drop (Scholz, 2002), and $r = 100$ km as characteristic of the rupture extent of large earthquakes, we find that $V_{p/d} \approx 0.8$–8 km per decade using $\zeta = \sqrt{2\pi}$. This range of migration velocities is consistent with the observations that typically find values on the order of several kilometers per decade.

As $V_{p/d} \approx \zeta A r / \Delta \tau$ and assuming a small variability of the parameters A and $\Delta \tau$ from one earthquake to the other, our model predicts that $V_{p/d} \propto r$ so that the aftershock migration velocities should scale with the size of the earthquake. To our knowledge, such a correlation has not been reported so far. This statement should be tested on a given fault where similar values of A and $\Delta \tau$ are more likely to be observed, comparing aftershock sequences corresponding to mainshock of different magnitudes, for instance on Japanese or Chilean megathrusts.

When applied to the aftershock sequence of the Tohoku-Oki earthquake, the simple scaling $V_{p/d} \approx \zeta A r / \Delta\tau$ predicted by our model can explain the fact that the aftershock migration velocities are larger in the along-strike direction than the along-dip direction, together with the lateral variations of the along-strike migration velocity (section 4.3). Assuming a linear decay of the stress drop over the rupture area (so that the gradient in Coulomb stress can be approximated by $\Delta\tau/r$) and weak variations of the A parameter with depth, the observed migration velocities are basically reflecting the geometric features of the coseismic rupture. This is unsurprising given the general observation that the aftershock zone scales with the magnitude of the coseismic rupture.

The complete expressions of the migration velocities are given in equations (11) and (14) for the along-strike and along-dip migrations. No approximation has been made when considering the along-strike migration. For the updip migration velocity, we have neglected in equation (14) the relative variations of the rheological parameter A with depth compare to the relative changes in coseismic Coulomb stress change. Doing so, we emphasize the effect of the mainshock by putting all depth dependence in ΔCFS. This is potentially a weak assumption, as the rupture process is likely to be influenced by the rheological (parameter A) or loading (parameter $\dot{\tau}$) conditions, keeping in mind that seismic rupture can be arrested when encountering rate strengthening regions (e.g., Kaneko et al., 2010). High gradients in Coulomb stress changes are thus expected in regions of high gradients in A parameter. Because the constraints on the variations of the A parameter with depth are weak even if some information has been reported in Frank et al. (2017) considering the Illapel aftershock sequence, we have decided to neglect this contribution. Nevertheless, one has to keep in mind that such gradient in A parameter might contribute to the along-dip migration velocities according to equation (14). Such a feature might, for instance, explain the fact that updip migration velocities are larger than the downdip ones (Figure 4). Indeed, according to equation (14), low gradients in the A parameter implies migration velocities larger than strong gradients of A. Based on Figure 4a of Frank et al. (2017) considering the Illapel aftershock sequence, A is found to be roughly constant from 0 to about 20 km while varying more significantly at greater depths (20–40 km). Based on equation (14), this would imply a faster migration velocity from 0–20 km than from 20–40 km, consistent with the observations in Figure 4.

Appendix A: Estimate of the Along-Strike and Updip Aftershock Migration Velocities

A1. Calculation of the Spatial Derivatives of the Slip Distribution

According to equations (6a)–(6c), the spatial derivatives of U with respect to the along-strike and updip distance x and z are given by

$$\frac{\partial U}{\partial x} = \frac{V_L t_r}{D} \frac{\partial D}{\partial x} \tag{A1a}$$

$$\frac{\partial U}{\partial z} = V_L t_r \left[\frac{1}{t_r} \frac{\partial t_r}{\partial z} \log D + \frac{1}{D} \frac{\partial D}{\partial z} \right] \tag{A1b}$$

With the use of equation (6a), equations (A1a) and (A1b) can be written as

$$\frac{\partial U}{\partial x} = \frac{V_L t_r}{D} \frac{\partial D}{\partial x} \tag{A2a}$$

$$\frac{\partial U}{\partial z} = \frac{U}{t_r} \frac{\partial t_r}{\partial z} + \frac{V_L t_r}{D} \frac{\partial D}{\partial z} \tag{A2b}$$

Using equation (6c), the spatial derivatives of D with respect to x and z are

$$\frac{\partial D}{\partial x} = \frac{1}{V_L} \frac{\partial V_+}{\partial x} \left[\exp\left(t/t_r\right) - 1 \right] \tag{A3a}$$

$$\frac{\partial D}{\partial z} = \frac{1}{V_L} \frac{\partial V_+}{\partial z} \left[\exp\left(t/t_r\right) - 1 \right] + \frac{V_+}{V_L} \exp\left(t/t_r\right) \left(-\frac{t}{t_r^2}\right) \frac{\partial t_r}{\partial z} \tag{A3b}$$

Equations (A3b) can be written as

$$\frac{\partial D}{\partial x} = \frac{V_+}{V_L} \exp\left(t/t_r\right) \left(\frac{1}{V_+} \frac{\partial V_+}{\partial x} \right) \left[1 - \exp\left(-t/t_r\right) \right] \tag{A4a}$$

$$\frac{\partial D}{\partial z} = \frac{V_+}{V_L} \exp\left(t/t_r\right) \left[\left(\frac{1}{V_+} \frac{\partial V_+}{\partial z}\right) \left[1 - \exp\left(-t/t_r\right)\right] - \frac{t}{t_r} \left(\frac{1}{t_r} \frac{\partial t_r}{\partial z}\right)\right] \tag{A4b}$$

Using Equations (6b) and (6c), equations (A4a) and (A4b) become

$$\frac{1}{D} \frac{\partial D}{\partial x} = \frac{V}{V_L} F \left(\frac{1}{V_+} \frac{\partial V_+}{\partial x}\right) \tag{A5a}$$

$$\frac{1}{D} \frac{\partial D}{\partial z} = \frac{V}{V_L} \left[F \left(\frac{1}{V_+} \frac{\partial V_+}{\partial z}\right) - \frac{t}{t_r} \left(\frac{1}{t_r} \frac{\partial t_r}{\partial z}\right)\right] \tag{A5b}$$

where the function F is defined as

$$F(z;t) = 1 - \exp\left(-t/t_r(z)\right) \tag{A6}$$

Using equations (A5a) and (A5a), equations (A2a) and (A2b) yield

$$\frac{\partial U}{\partial x} = F t_r V \left(\frac{1}{V_+} \frac{\partial V_+}{\partial x}\right) \tag{A7a}$$

$$\frac{\partial U}{\partial z} = V \left[\frac{1}{t_r} \frac{\partial t_r}{\partial z} \left(\frac{U}{V} - t\right) + F t_r \left(\frac{1}{V_+} \frac{\partial V_+}{\partial z}\right)\right] \tag{A7b}$$

As equation (A3a) can be written as $\log(V_+/V_L) = \frac{\Delta \mathrm{CFS}}{A}$, the spatial derivatives of V_+ are given by

$$\frac{1}{V_+} \frac{\partial V_+}{\partial x} = \frac{1}{A} \frac{\partial \Delta \mathrm{CFS}}{\partial x} \tag{A8a}$$

$$\frac{1}{V_+} \frac{\partial V_+}{\partial z} = \frac{1}{A} \left[\frac{\partial \Delta \mathrm{CFS}}{\partial z} - \left(\frac{1}{A} \frac{\partial A}{\partial z}\right) \Delta \mathrm{CFS}\right] \tag{A8b}$$

Combining equations (A7a) and (A7b) with (A8a) and (A8b) gives

$$\frac{\partial U}{\partial x} = \frac{F t_r V}{A} \frac{\partial \Delta \mathrm{CFS}}{\partial x} \tag{A9a}$$

$$\frac{\partial U}{\partial z} = V \left[\left(\frac{1}{t_r} \frac{\partial t_r}{\partial z}\right) \left(\frac{U}{V} - t\right) + \frac{F t_r}{A} \frac{\partial \Delta \mathrm{CFS}}{\partial z} - F t_r \left(\frac{1}{A} \frac{\partial A}{\partial z}\right) \frac{\Delta \mathrm{CFS}}{A}\right] \tag{A9b}$$

A2. Along-Strike Migration Velocity

According to equation (9), the along-strike aftershock migration velocity is given by

$$V_p^x = \frac{-V}{\frac{\partial U}{\partial x}} = \frac{A}{F t_r} \times \left(-\frac{\partial \Delta \mathrm{CFS}}{\partial x}\right)^{-1} \tag{A10}$$

where equation (A9a) has been used.

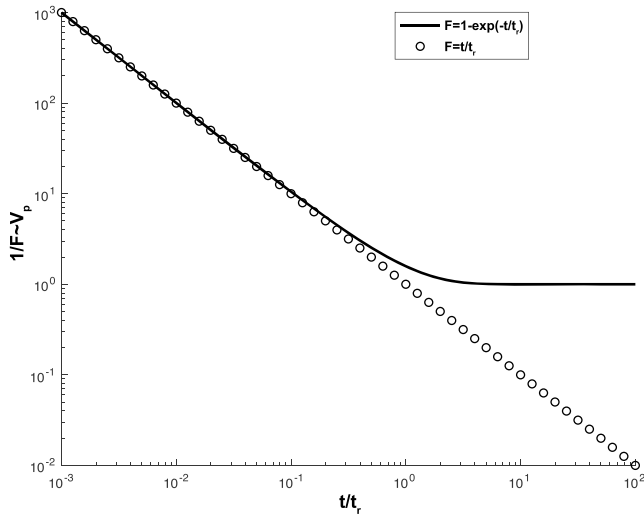The function F defined in equation (A6) has the following asymptotic behavior

$$\lim_{t \to 0} F = \frac{t}{t_r} \tag{A11a}$$

$$\lim_{t \to +\infty} F = 1 \tag{A11b}$$

In the limit of small relaxation times ($t \ll t_r$), equation (A10) becomes, after use of (A11a),

$$V_p^x = \frac{A}{t} \times \left(-\frac{\partial \Delta \mathrm{CFS}}{\partial x}\right)^{-1} \tag{A12}$$

Equation (A12) shows that the migration velocity decays as $1/t$ in the early postseismic phase.

Figure A1. Temporal evolution $1/F \propto V_p$ of the along-strike aftershock migration. The approximation $V_p^x \propto 1/t$ corresponding to Equation (A11a) ceases to be valid when t approaches t_r. At latter times, the full expression of equation (12) predicts a constant value of the migration velocity corresponding to equation (A11b).

In the limit of large relaxation times ($t \gg t_r$), equation (A10) becomes, after use of (A11b),

$$V_p^x = V_p^{x\infty} = \dot{\tau} \times \left(-\frac{\partial \Delta \text{CFS}}{\partial x} \right)^{-1} \tag{A13}$$

where equation (2a) has been used.

Equation (A13) shows that the migration velocity reaches a constant finite value at large times, whereas the early time approximation of equation (A12) predicts that V_p would reach arbitrary small values.

Figure A1 shows $1/F$ (a proxy for the temporal evolution of V_p^x) as a function of time, considering the full expression of F defined in equation (A6) and the approximation $F \approx t/t_r$ corresponding to the limit $t \ll t_r$. The short time approximation starts to deviate from the full expression as t approaches the duration t_r of the aftershock sequence.

A3. Updip Migration Velocity

According to equation (10), the updip aftershock migration velocity is given by

$$V_p^z = \frac{-V}{\frac{\partial U}{\partial z}} = -\left[\left(\frac{1}{t_r}\frac{\partial t_r}{\partial z} \right)\left(\frac{U}{V} - t \right) + \frac{Ft_r}{A}\frac{\partial \Delta \text{CFS}}{\partial z} - Ft_r\left(\frac{1}{A}\frac{\partial A}{\partial z} \right)\frac{\Delta \text{CFS}}{A} \right]^{-1} \tag{A14}$$

where equation (A9b) has been used.

The spatial derivative of $t_r = A/\dot{\tau}$ with respect to z is given by

$$\frac{1}{t_r}\frac{\partial t_r}{\partial z} = \frac{1}{A}\frac{\partial A}{\partial z} - \frac{1}{\dot{\tau}}\frac{\partial \dot{\tau}}{\partial z} \tag{A15}$$

Introducing equation (A15) in (A14) gives

$$V_p^z = -\left[\left(\frac{1}{A}\frac{\partial A}{\partial z} - \frac{1}{\dot{\tau}}\frac{\partial \dot{\tau}}{\partial z} \right)\left(\frac{U}{V} - t \right) + \frac{Ft_r}{A}\frac{\partial \Delta \text{CFS}}{\partial z} - Ft_r\left(\frac{1}{A}\frac{\partial A}{\partial z} \right)\frac{\Delta \text{CFS}}{A} \right]^{-1} \tag{A16}$$

which can be rearranged as

$$V_p^z = \left\{ \left(\frac{1}{A}\frac{\partial A}{\partial z} \right)\left[Ft_r\frac{\Delta \text{CFS}}{A} - \left(\frac{U}{V} - t \right) \right] + \left(\frac{1}{\dot{\tau}}\frac{\partial \dot{\tau}}{\partial z} \right)\left(\frac{U}{V} - t \right) + \frac{Ft_r}{A}\left(\frac{-\partial \Delta \text{CFS}}{\partial z} \right) \right\}^{-1} \tag{A17}$$

The function D defined in equation (6c) has the following asymptotic behavior

$$\lim_{t \to 0} D = 1 + \frac{t}{t_r}\frac{V_+}{V_L} \tag{A18a}$$

$$\lim_{t \to +\infty} D = \frac{V_+}{V_L}\exp\left(\frac{t}{t_r} \right) \tag{A18b}$$

so that the asymptotic behavior of U given in equation (6a) is given by

$$\lim_{t \to 0} U = V_+ t \tag{A19a}$$

$$\lim_{t \to +\infty} U = V_L t \tag{A19b}$$

Using equations (A18a) and (6b), the asymptotic behavior of V is given by

$$\lim_{t \to 0} V = V_+ \tag{A20a}$$

$$\lim_{t \to +\infty} V = V_L \tag{A20b}$$

Therefore, considering the asymptotic behavior of U and V given in equations (A19a) and (A19b), and (A20a) and (A20b), we find that to a first-order approximation $\frac{U}{V} - t \approx 0$ both at small and large relaxation times. Neglecting the $\frac{U}{V} - t$ terms in equation (A17) leads to

$$V_p^z = \frac{A}{Ft_r} \times \left[\left(\frac{1}{A} \frac{\partial A}{\partial z} \right) \Delta\text{CFS} + \left(\frac{-\partial \Delta\text{CFS}}{\partial z} \right) \right]^{-1} \tag{A21}$$

Using equation (A11a), equation (A21) gives

$$V_p^z \approx \frac{A}{t} \times \left[\left(\frac{1}{A} \frac{\partial A}{\partial z} \right) \Delta\text{CFS} + \left(\frac{-\partial \Delta\text{CFS}}{\partial z} \right) \right]^{-1}, \; t \ll t_r \tag{A22}$$

while equation (A11b) leads to

$$V_p^z \approx \dot{\tau} \times \left[\left(\frac{1}{A} \frac{\partial A}{\partial z} \right) \Delta\text{CFS} + \left(\frac{-\partial \Delta\text{CFS}}{\partial z} \right) \right]^{-1}, \; t \gg t_r \tag{A23}$$

Appendix B: Estimate of the Along-Strike and Along-Dip Positions

We start by considering all the events that have occurred during the postseismic period with moment-magnitude $M_w > M_c$, where M_c is a threshold magnitude greater than the magnitude of completeness of the earthquake catalog in the postseismic period. We consider a threshold magnitude M_c of $M_c = 2$ for the Tohoku-Oki earthquake (93,331 events).

Because aftershocks are triggered in our model when a given level of slip is reached on the fault plane, we extract from the aftershock population all the events that are located less than 20 km away from the fault plane. The fault geometry considered for the Tohoku-Oki earthquake comes from Hayes et al. (2012).

We next convert the longitude and latitude coordinates to Cartesian coordinates expressed in a reference frame R with origin O located at the mainshock epicenter and which basis vectors $(\vec{i}, \vec{j}, \vec{k})$ are respectively oriented along the east, north, and updip vertical axis. Let us consider a given aftershock occurring at point M and which position vector $\overrightarrow{OM}$ is given by

$$\overrightarrow{OM} = x\vec{i} + y\vec{j} + z\vec{k} \tag{B1}$$

To study the aftershock migration along the fault plane, we consider a reference frame R', which origin is the mainshock hypocenter O' and which basis vectors $(\vec{s}, \vec{u}, \vec{n})$ are oriented respectively along the mean fault strike, mean updip, and mean normal directions to the fault plane. In this reference frame, the position of the aftershock occurring at point M is given by

$$\overrightarrow{O'M} = x'\vec{s} + y'\vec{u} + z'\vec{n} \tag{B2}$$

where $\vec{s}$, $\vec{u}$, and $\vec{n}$ are respectively the unit vectors oriented along the mean fault strike, updip, and normal axis of the mean fault plane. Since $\overrightarrow{O'M} = \overrightarrow{O'O} + \overrightarrow{OM}$, equation (B2) can be written as

$$\overrightarrow{O'M} = x\vec{i} + y\vec{j} + (z + d_e)\vec{k} \tag{B3}$$

where equation (B1) has been used together with $\overrightarrow{O'O} = d_e\vec{k}$, where d_e is the depth of the mainshock, equal to $d_e = -23.74$ km for the Tohoku-Oki hypocenter.

The coordinates (x', y', z') are obtained evaluating the following scalar products:

$$x' = \overrightarrow{O'M}.\vec{s} \tag{B4a}$$

$$y' = \overrightarrow{O'M}.\vec{u} \tag{B4b}$$

$$z' = \overrightarrow{O'M}.\vec{n} \tag{B4c}$$

where the mean strike, updip, and normal vectors $\vec{s}$, $\vec{u}$, and $\vec{n}$ are expressed in the reference frame R.

References

Chatelain, J., Cardwell, R., & Isacks, B. (1983). Expansion of the aftershock zone following the Vanuatu (New Hebrides) earthquake on 15 July 1981. *Geophysical Research Letters*, *10*, 385–388.

Frank, W. B., Poli, P., & Perfettini, H. (2017). Mapping the rheology of the central chile subduction zone with aftershocks. *Geophysical Research Letters*, *44*, 5374–5382. https://doi.org/10.1002/2016GL072288

Hayes, G., Wald, D., & Johnson, R. (2012). Tslab1.0: A three-dimensional model of global subduction zone geometries. *Journal of Geophysical Research*, *117*, B01302. https://doi.org/10.1029/2011JB008524

Henry, C., & Das, S. (2001). Aftershock zones of large shallow earthquakes: Fault dimensions, aftershock area expansion and scaling relations. *Geophysical Journal International*, *147*, 272–293.

Kaneko, Y., Avouac, J., & Lapusta, N. (2010). Towards inferring earthquake patterns from geodetic observations of interseismic coupling. *Nature Geoscience*, *3*, 363–369. https://doi.org/10.1038/ngeo843

Kato, A., & Obara, K. (2014). Step-like migration of early aftershocks following the 2007 m_w 6.7 Noto-Hanto earthquake, Japan. *Geophysical Research Letters*, *41*, 3864–3869. https://doi.org/10.1002/2014GL060427

Meng, X., & Peng, Z. (2016). Increasing lengths of aftershock zones with depths of moderate-size earthquakes on the San Jacinto Fault suggests triggering of deep creep in the middle crust. *Geophysical Journal International*, *204*, 250–261. https://doi.org/10.1093/gji/ggv445

Nanjo, K., Ishibe, T., Tsuruoka, H., Schorlemmer, D., Ishigaki, Y., & Hirata, N. (2010). Analysis of the completeness magnitude and seismic network coverage of Japan. *Bulletin of the Seismological Society of America*, *100*, 3261–3268. https://doi.org/10.1785/0120100077

Obana, K., Takahashi, T., Kaiho, Y., Kodaira, S., Yamashita, M., Sato, T., & Nakamura, T. (2014). Distribution and migration of aftershocks of the 2010 m_w 7.4 Ogasawara Islands intraplate normal-faulting earthquake related to a fracture zone in the pacific plate. *Geochemistry, Geophysics, Geosystems*, *15*, 1363–1373. https://doi.org/10.1002/2014GC005246

Peng, Z., & Zhao, P. (2009). Migration of early aftershocks following the 2004 Parkfield earthquake. *Nature Geoscience*, *2*, 877–881.

Perfettini, H., & Avouac, J.-P. (2004). Postseismic relaxation driven by brittle creep: A possible mechanism to reconcile geodetic measurements and the decay rate of aftershocks, application to the chi-chi earthquake, taiwan. *Journal of Geophysical Research*, *109*, B02304. https://doi.org/10.1029/2003JB002488

Perfettini, H., & Avouac, J.-P. (2007). Modelling afterslip and aftershocks following the 1992 Landers earthquake. *Journal of Geophysical Research*, *112*, B07409. https://doi.org/10.1029/2006JB004399

Perfettini, H., & Avouac, J.-P. (2014). The seismic cycle in the area of the 2011 m_w 9.0 Tohoku-Oki earthquake. *Journal of Geophysical Research: Solid Earth*, *119*, 4469–4515. https://doi.org/10.1002/2013JB010697

Perfettini, H., Avouac, J., Tavera, H., Kositsky, A., Nocquet, J., Bondoux, F., et al. (2010). Seismic and aseismic slip on the central Peru megathrust. *Nature*, *465*, 78–81. https://doi.org/10.1038/nature09062

Perfettini, H., Frank, W., Marsan, D., & Bouchon, M. (2018). A model of aftershock migration driven by afterslip. *Geophysical Research Letters*, *45*, 2283–2293. https://doi.org/10.1002/2017GL076287

Scholz, C. H. (2002). *The Mechanics of Earthquakes and Faulting*. New York: Cambridge University Press.

Tajima, F., & Kanamori, H. (1985). Global survey of aftershock area expansion patterns. *Physics of the Earth and Planetary Interiors*, *40*, 77–134.

Tang, C.-C., Lin, C.-H., & Peng, Z. (2014). Spatial-temporal evolution of early aftershocks following the 2010 m_l 6.4 Jiashian earthquake in southern Taiwan. *Geophysical Journal International*, *199*, 1772–1783.

Wei, S., Graves, R., Helmberger, D., Avouac, J.-P., & Jiang, J. (2012). Sources of shaking and flooding during the Tohoku-Oki earthquake: A mixture of rupture styles. *Earth and Planetary Science Letters*, *333-334*, 91–100.

Wesson, R. L. (1987). Modelling aftershock migration and afterslip of the San Juan Bautista, California, earthquake of October 3, 1972. *Tectonophysics*, *144*, 215–229.